RSC Advances

PAPER

View Article Online
View Journal | View Issue

Cite this: *RSC Adv.*, 2023, **13**, 17362

CdO decorated CdS nanorod for enhanced photocatalytic reduction of CO_2 to CO†

Zhe Zhang, *[ab] Fanhao Kong,[c] Bizhen Yuan,[ab] Yinnian Liao,[ab] Xiue Ren[ab] and Yu Hou[ab]

Received 25th April 2023
Accepted 31st May 2023

DOI: 10.1039/d3ra02739b

rsc.li/rsc-advances

Solar-driven CO_2 reduction into fuels and sustainable energy has attracted increasing attention around the world. However, the photoreduction efficiency remains low due to the low efficiency of separation of electron–hole pairs and high thermal stability of CO_2. In this work, we prepared a CdO decorated CdS nanorod for visible light driven CO_2 reduction. The introduction of CdO facilitates the photoinduced charge carrier separation and transfer and acts as an active site for adsorption and activation of CO_2 molecules. Compared with pristine CdS, CdO/CdS exhibits a nearly 5-fold higher CO generation rate (1.26 mmol g^{-1} h^{-1}). *In situ* FT-IR experiments indicated that CO_2 reduction on CdO/CdS may follow a COOH* pathway. This study reports the pivotal effect of CdO on photogenerated carrier transfer in photocatalysis and on CO_2 adsorption, which provides a facile way to enhance photocatalytic efficiency.

Introduction

Photocatalytic reduction of CO_2 by sunlight is a sustainable energy economy because this process is promising to store solar energy in the chemical bonds and produce useful chemicals and fuels such as CO.[1–4] Though a great amount of work has been done during the past several decades, the photoreduction efficiency remains low due to the low efficiency of separation of electron–hole pairs and the high thermal stability of CO_2.[5–9] Multifarious strategies have been developed to promote charge-separation, such as the construction of heterojunctions,[10–13] heteroatom doping,[14–16] and band-structure engineering.[17–24]

Moreover, water is the most preferred and widely used reductant for CO_2 reduction, and the photo splitting of water to generate H_2 occurs in the photoreduction of CO_2. CO_2 is one of the most stable and chemically inert molecules. The free energy change of the conversion of CO_2 to CO is 257 kJ mol^{-1}, which is higher than that of H_2O to H_2 (237 kJ mol^{-1}).[25,26] The competitive consumption of the photoinduced electrons to reduce CO_2 or protons limits the CO_2 reduction efficiency.[27–30] Many reported works for CO_2 reduction generate more H_2 than CO_2 reduction products. Efforts have been made to prevent the hydrogen generation and promote CO production.[31–33] To ameliorate the efficiency of photocatalytic reduction of CO_2, efforts should be made to explore catalysts that could simultaneously efficiently separate hole–electron pairs, selectively activate CO_2, and prohibit the hydrogen generation.

Recently, CdS has been frequently reported in various photocatalytic systems. However, its photocatalytic activity is poor due to its high recombination rate of photogenerated electron–hole pairs. To enhance its photoactivity, efforts have been put to modify the composition and structure of CdS, such as N-doped graphene grown on CdS hollow spheres,[16] anchoring of a molecular Ni catalyst on CdS,[34] coating CdS with ZIF-8 to form a core–shell structure,[17] decorating CdS with Pt nanoparticle,[35] Co complex assembled by CdS.[36]

In this work, CdS nanorod is used as the visible light responsive photocatalyst. CdO was grown on CdS *via* plasma treatment. The as-prepared CdO/CdS is effective for the photocatalytic reduction of CO_2 under visible light irradiation at room temperature. Compared with pristine CdS, this CdO/CdS catalyst exhibits higher reaction rate, nearly 5-fold higher CO generation (1.26 mmol g^{-1} h^{-1}) and suppresses H_2 generation rate (0.24 mmol g^{-1} h^{-1}). This study reveals the promoting effect of CdO on suppressing recombination of photogenerated carriers and on CO_2 adsorption, which provides a novel method to enhance photocatalytic efficiency.

Results and discussion

Pristine CdS nanorod was prepared according to the literature.[37,38] The characterization of the XRD patterns of CdS could be well indexed to hexagonal wurtzite structure with good crystallinity (JCPDS no. 41-1049).[39] The CdO/CdS catalyst was prepared as Scheme S1† by H_2 plasma treatment, and then

[a]*School of Applied Chemistry and Materials, Zhuhai College of Science and Technology, Zhuhai, 519040, Guangdong, China. E-mail: zhzh@zcst.edu.cn*

[b]*Faculty of Comprehensive Health Industry, Zhuhai College of Science and Technology, Zhuhai, 519040, Guangdong, China*

[c]*School of Chemistry, Dalian University of Technology, Dalian, 116024, Liaoning, China*

† Electronic supplementary information (ESI) available: Full detailed experiment, characterizations of catalysts, and reaction data. See DOI: https://doi.org/10.1039/d3ra02739b

treated by air oxidation at ambient temperature. After H_2 plasma treatment, sulfur atoms are first removed, and then a small amount of CdO was formed followed by air oxidation as shown by the appearance of CdO (200) peak at 38.3° (JCPDS no. 65-2908), as confirmed by transition electron microscopy (TEM) (Fig. 1a and b). TEM images of CdO/CdS show that the surfaces of CdS nanorods are rough compared to the pristine CdS, and many round particles emerged at the surface. These particles were then investigated by HRTEM images (Fig. 1b). As presented, the three kinds of lattice fringes with fringe pacing of 0.271, 0.23, and 0.166 nm are consistent with the (111), (200), and (220) lattice plane of CdO, respectively. And the lattice fringe spacing of 0.336, and 0.36 nm are attributed to the (002), and (100) lattice plane of CdS, respectively. These results clearly indicate that CdO particles have been constructed on the surface of CdS after plasma treatment. The Cd 3d peaks of CdO/CdS red shift 1 eV compared to that of CdS samples, resulting from CdO environments on the CdS surface.[40,41] Raman is useful for the characterization of CdO species. Raman measurements further provided evidence for the formation of CdO on the surface of CdS (Fig. 1c). Vibrational bands at 305 cm^{-1} and 595 cm^{-1} are assigned to scattering and double scattering on the longitudinal optical phonon of CdS (LO and 2LO), respectively.[40–42] The broad and intense structure spanning from 300 to 390 cm^{-1} could be attributed to CdO by comparison to a reference spectrum of CdO.[43]

The presence of CdO at the CdS surface changes the energy band structure. The VB potentials of pristine CdS and CdO/CdS are analyzed. As shown in Fig. 1e, the VB potentials of CdO/CdS shifts positive to 1.49 eV, which means the oxidizing power of CdO/CdS is higher than CdS. The band gap of CdO/CdS was nearly the same as pristine CdS (Fig. S1 and S2†). In this case, the electrons can be more easily photoexcited from VB to the conduction band.

The separation and transfer of charge carriers were further examined through photoluminescence (PL) emission spectra, electrochemical impedance spectroscopy (EIS), and transient photocurrent responses. As shown in Fig. 2, the PL emission spectra exhibit a strong peak at about 510 nm, which is attributed to the essential excitonic emission of CdS,[44] in agreement with its band gap energy, which was confirmed by the UV-vis diffuse reflectance adsorption spectra. CdO/CdS retains the light adsorption consistent with CdS, and the spectrum is slightly broadened, with a bandgap of *ca.* 2.40 eV (Fig. S2†). CdO/CdS shows a decreased PL intensity in comparison with CdS, demonstrating that CdO/CdS inhibits the photogenerated carrier recombination. The lifetime of the two samples were then calculated *via* a photoelectron experiment in Fig. S3,†

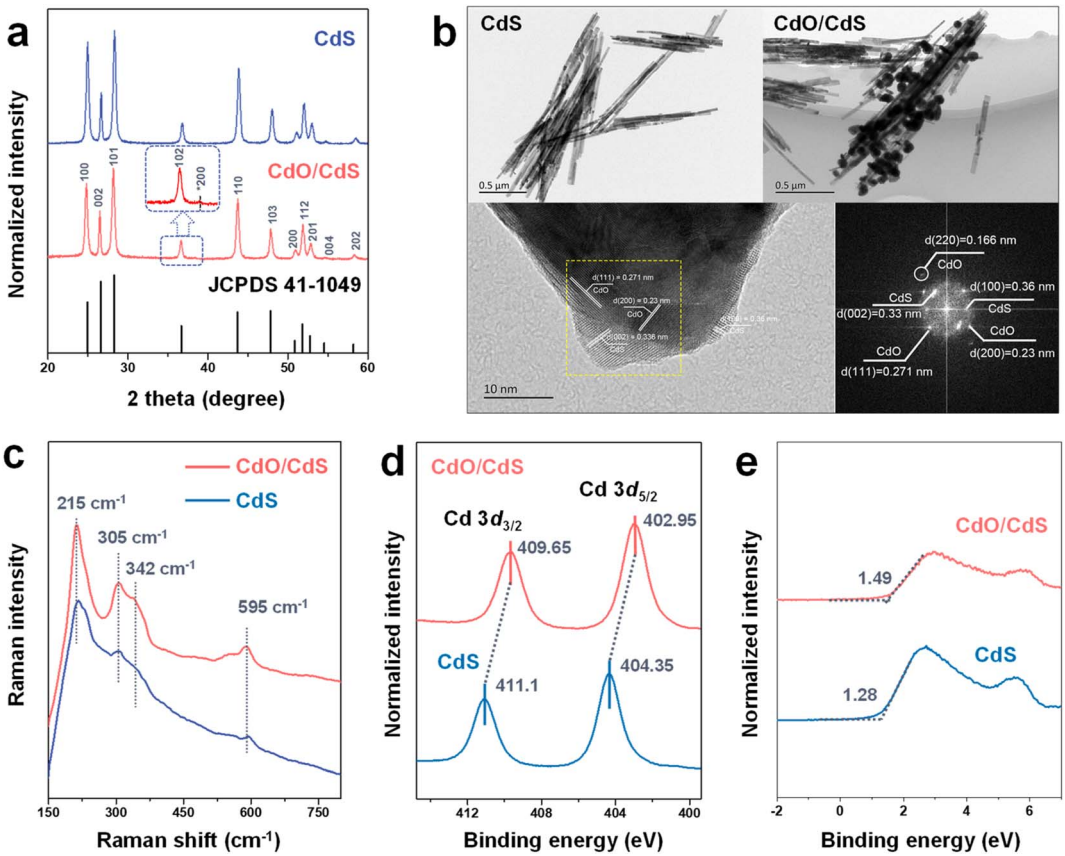

Fig. 1 Characterizations of CdS samples. (a) XRD patterns of CdS and CdO/CdS. (b) TEM and HRTEM images of CdS and CdO/CdS. (c) Raman spectra of CdS and CdO/CdS at an excitation wavelength of 785 nm. (d) XPS analysis of the Cd (3d) region of CdS and CdO/CdS. (e) Valance band spectra of CdS and CdO/CdS.

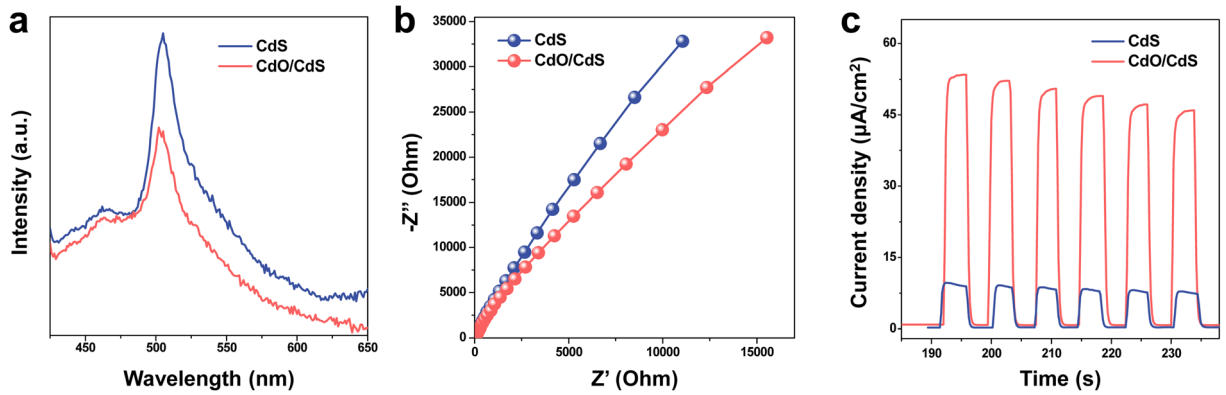

Fig. 2 Photoelectrical properties of catalysts. (a) Photoluminescence emission spectra, (b) EIS Nyquist plots, and (c) transient photocurrent responses of CdS and CdO/CdS.

which demonstrate that the lifetime of photogenerated electrons of CdO/CdS is longer than that of CdS in accordance with the PL spectra. On the other hand, the current density *vs.* time curves consist of six similar trapezoids, and the start and end of each curve edge demonstrate that the photocurrent was fast generated with light irradiation and was rapidly vanished when light was stopped. The photocurrent density of CdO/CdS is notably higher than that of CdO/CdS with several on–off cycles of light irradiation (Fig. 2b), which means a better photoinduced carrier separation. Electrochemical impedance spectroscopy (EIS) was then carried out for further investigation. The Nyquist plot of CdO/CdS presents a reduction in the radius of the semi cycle arc compared to CdS, indicating a more efficient interfacial charge migration. These results illustrate that the photoexcited electrons and holes of CdO/CdS were separated and transmitted quickly and their recombination was inhibited.

We then investigated the catalytic performance of CdO/CdS in the CO_2 photocatalytic reduction under visible light (455 nm LEDs) irradiation. Gas chromatography (GC) was employed to identify and quantify the gas product, where CO was detected as the solo reduction product and no other detectable reduction liquid products by high performance liquid chromatography (HPLC). A series of semiconductor photocatalysts were screened in CO_2 photocatalytic reduction to CO in MeCN–water (9 : 1) solution (Fig. S4†). Most of the widely used catalysts, such as Nb_2O_5, Bi_2WO_6, P25, Bi_2O_3, CeO_2 were inactive for this reaction. CdS was active and generated 3.4 mmol $g_{cat.}^{-1}$ of CO and 9.1 mmol $g_{cat.}^{-1}$ of H_2. After plasma treatment of CdS, the activity was greatly improved. CdO/CdS produced 15.1 mmol $g_{cat.}^{-1}$ of CO, nearly 5 times over CdS. To exclude that CO comes from MeCN solvent, we performed the photoreaction in the absence of CO_2. When CO_2 was replaced with argon, CO was undetected. Then we performed the time profile of photocatalytic conversion from CO_2 to CO over CdS and CdO/CdS. As the reaction proceeds, the yield of CO over CdO/CdS increases, which is 6 times that over pristine CdS after 6 h (Fig. 3a). And the H_2 productivity over CdO/CdS is lower than that over pristine CdS, which is 0.26 times of the latter (Fig. 3b). CO_2 reduction and H_2 generation are competitive reactions, and they both need photo-generated electrons. These results

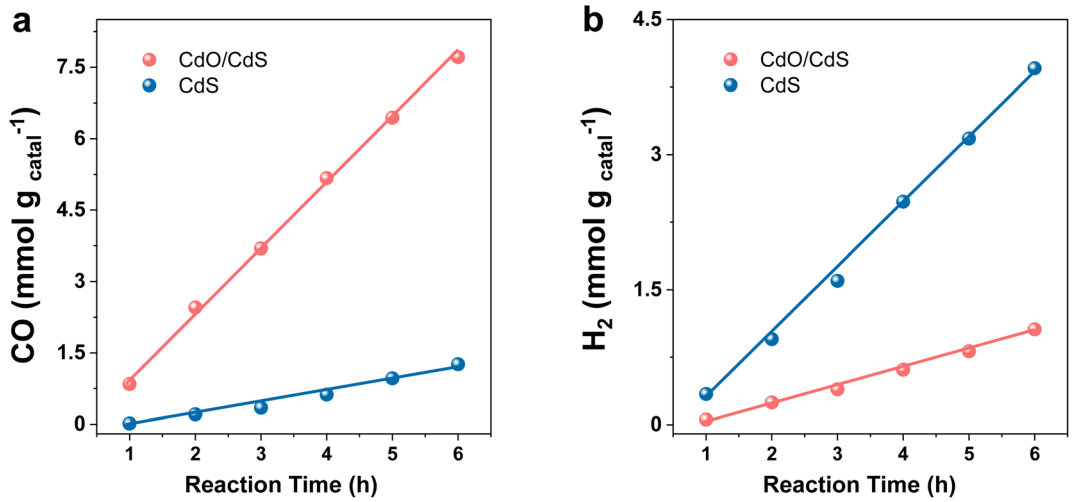

Fig. 3 Time profile of photocatalytic reduction of CO_2 to CO over CdS and CdO/CdS catalysts under standard reaction conditions. (a) CO productivity; (b) H_2 productivity.

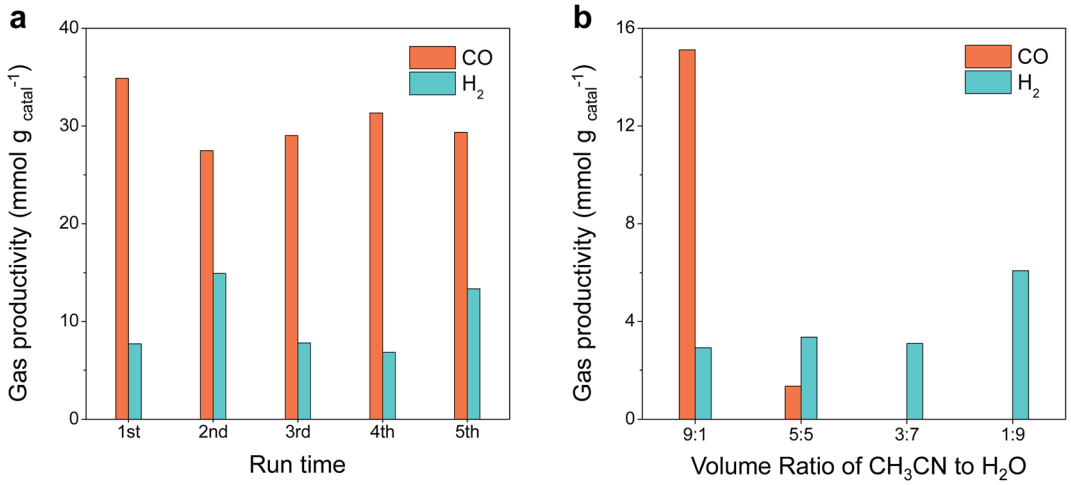

Fig. 4 The photocatalytic performance of CdO/CdS catalyst. (a) Catalyst reusability under standard reaction conditions in 24 h. (b) Solvent effect under standard reaction conditions.

showed that CdO/CdS tended to the selective reduction of CO_2 reduction over hydrogen evolution. The amount of CO and H_2 was nearly linearly increased. The catalyst is stable and could be reused for at least 5 times with no apparent loss of activity (Fig. 4a). We also investigated the solvent effect on the reaction, and when MeCN/H_2O ratio was 9 : 1, CO generated most (Fig. 4b).

To further elucidate the reason why CdO/CdS favors CO_2 reduction, we then investigate the adsorption ability of the catalysts towards CO_2. After photoirradiation with 450 nm laser in the presence of CO_2, no apparent peaks were observed, indicating the interaction on the catalyst surface is very weak for pristine CdS. On the contrary, CdO/CdS behaved better CO_2 adsorption ability. Several peaks could be observed (Fig. 5a). The peaks at 1688 and 1383 cm^{-1} could be assigned to the bidentate bicarbonate (b-HCO^{3-}) and bidentate carbonate (b-CO_3^{2-}), respectively.[45] And the peaks at 1586 and 1262 cm^{-1} could be assigned to the formate (COO^-), suggesting that CO_2

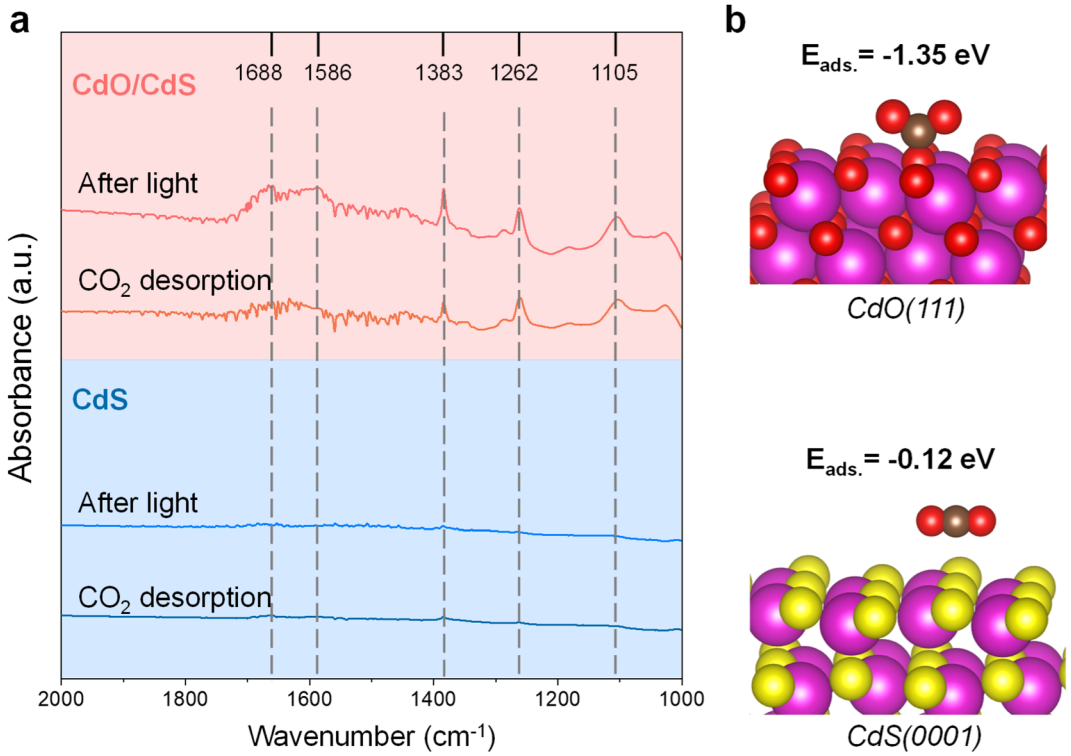

Fig. 5 CO_2 adsorption to CdS samples. (a) FTIR absorbance spectra of CO_2 adsorption to CdO/CdS and CdS. (b) CO_2 adsorption energy to CdO (111) and CdS (0001).

reduction could follow a COOH* pathway.[46] After evacuation, these peaks still exist though some of which slightly weakened, while no apparent change happened over pristine CdS. These results demonstrate that CdO/CdS had better CO_2 adsorption ability. We also calculate the adsorption energy of CO_2 to CdO (111) and CdS (0001). The adsorption energy of CO_2 to CdO is higher than to CdS, which showed that the introduction of CdO facilitate the activation of CO_2 (Fig. 5b).

Conclusion

In summary, we developed a method to generate CdO on CdS *via* H_2 plasma treatment then air oxidation. Compared with pristine CdS, CdO/CdS exhibits nearly 5-fold higher CO generation rate (1.26 mmol g^{-1} h^{-1}) and 0.32-fold lower H_2 generation (0.24 mmol g^{-1} h^{-1}) in CO_2 photocatalytic reduction. The CdO/CdS is stable and could be used for at least five times without apparent loss of activity. Detailed studies demonstrate that CdO could facilitate separation of electron–hole pairs and could promote CO_2 adsorption. The present work reports the pivotal effect of CdO on CO_2 photocatalytic reduction, which provides a novel and facile method for increasing photocatalytic efficiency.

Experimental section

Materials

$Cd(NO_3)_2 \cdot 4H_2O$ (99%) was purchased from Shanghai Macklin Biochemical Co., Ltd. Thiourea (99%) and (±)1-phenylethanol (98%) were purchased from Shanghai Aladdin Bio-Chem Technology Co., Ltd. Ethylenediamine (99%) and acetonitrile (99%) were purchased from Damao Chemical Reagent Factory. All the reagents were used as received without further purification.

Preparation of catalysts

CdS nanorods were synthesized by a modified solvothermal method according to the literature. In a typical procedure, 4.62 g of cadmium nitrate and 4.62 g of thiourea were placed in a Teflon-lined steel chamber and filled with ethylenediamine, followed by 160 °C treatment for 24 hours. After cooling to room temperature, the resulting solid products were collected by systematic centrifugation, washed with deionized water. The products were then dried at 60 °C overnight. CdS nanorods were obtained finally as a yellow powder. The as-prepared CdS nanorods were then treated by radio-frequency excited plasma at room temperature for 20 minutes to afford CdO/CdS when the vacuum was kept around 0.2 mbar with a flow of H_2 at 10 mL min^{-1}, and the power was kept as 200 W. Then the samples were then kept with a flow of air to normal pressure and room temperature to finally afford CdO/CdS.

Characterizations

Crystalline information was measured by powder X-ray diffraction (XRD) patterns, conducted on a PANalytical X-Pert PRO diffractometer by using Cu Kα radiation at 40 kV and 20 mA. Continuous scans were in the 2θ range from 10°–80°. The surface structure of obtained catalysts was identified by X-ray photoelectron spectroscopy (XPS) analyses, performed at Thermo Fischer, ESCALAB Xi+. The binding energy was referenced to the C 1s peak at 284.80 eV. The catalyst morphology characteristics were observed by STEM images using a Titan G2 60-300. UV-vis DRS were recorded on a UV-vis spectrophotometer (UV-2600) at room temperature in the range of 300–900 nm with $BaSO_4$ as the background. Raman spectra were obtained at ExR610-PT7 at an excitation of 785 nm. Photoluminescence (PL) experiments were conducted on a Photon Technology International QM 400 Fluorescence Spectrophotometer. The excitation wavelength was 400 nm obtained by using a xenon lamp as the excitation source at room temperature. The electrochemical tests were conducted on an electrochemical workstation (Corrtest CS2350H). A three-electrode system with a platinum-plate electrode as the counter electrode and a saturated calomel electrode (SCE) as the reference electrode was used for measurements. Na_2SO_4 (0.5 M) was used as the electrolyte solution.

Reaction procedure and product analysis

The reaction was carried out in homemade LED photoreactors. Typically, 5 mg of catalyst and 0.1 mL of triethylamine were added into 1 mL of solvent in a 6.5 mL of quartz tube reactor, then the system was completely replaced with CO_2 before sealed with a cap. For the standard reaction conditions, 0.9 mL of CH_3CN, 0.1 mL of H_2O were used as solvent and reacted for 12 h. This quartz tube reactor could stand up 0.5 MPa pressure. The quartz tube was then irradiated with 455 nm LED light (18 W, 155 mW cm^{-2}) *via* side irradiation. The reaction temperature was kept between 25 and 35 °C. After the reaction, gas-phase products were analyzed by gas chromatography (GC) equipped with a TCD detector and TDX-01 column.

Adsorption FTIR

The CO_2 adsorption FTIR spectra were recorded using Thermo Scientific Nicolet iS10 IR spectrometer. The spectra of the adsorbed CO_2 molecules have subtracted the spectra of the samples before the adsorption. CO_2-adsorption FTIR spectra were conducted as follows: the CdS samples were placed in a homemade IR cell and evacuated ($P < 10^{-3}$ Pa) at 423 K for 0.5 h. Then, CO_2 was introduced into the cell at 303 K and left for 0.5 h. The cell was then evacuated for 0.5 h ($P < 10^{-2}$ Pa) to remove the physically adsorbed CO_2. Then CO_2 vapor was again introduced into the cell at 303 K and left for 0.5 h upon photoirradiation with 450 nm laser (300 mW cm^{-2}). The cell was then evacuated for 0.5 h ($P < 10^{-2}$ Pa) to remove the physically adsorbed CO_2.

DFT calculation settings

All of the first-principles electronic structure calculations were carried out using the Vienna *Ab initio* Simulation Package (VASP),[47] one density functional theory implementation. The exchange–correlation potential was described by the Perdew–Burke–Ernzerhof (PBE)[48] formulation of the generalized

gradient approximation (GGA). The ion–electron interactions were represented by the projector augmented wave (PAW)[49] method. A plane wave basis set with an energy cutoff of 400 eV was used. The *k*-point sampling was performed using the Monkhorst–Pack scheme.[50] The electronic self-consistent minimization was converged to 10^{-5} eV, and the geometry optimization was converged to −0.02 eV. The lattice constants of CdS were optimized to be $a = 4.200$ Å, $b = 4.191$ and $c = 6.817$ Å, in good agreement with the experimental constants, $a = 4.14$ Å and $c = 6.72$ Å.[37,44,51] We used them to build a $(2 \times 2\sqrt{3})$ CdS (001) slab with 10 atomic layers and a vacuum of 15 Å. Atoms in the bottom 6 atomic layers were fixed to their bulk positions, while the rest were allowed to fully relax. A $4 \times 2 \times 1$ *k*-point mesh was used. The lattice constants of CdO were optimized to be $a = b = c = 4.695$ Å. We used them to build a (1×2) CdS (001) slab with 5 atomic layers and a vacuum of 15 Å. Atoms in the bottom 3 atomic layers were fixed to their bulk positions, while the rest were allowed to fully relax. A $4 \times 2 \times 1$ *k*-point mesh was used.

Conflicts of interest

The authors declare no competing interests.

Acknowledgements

This work was supported by the National Natural Science Foundation of China (22002011), Research Ability Improvement Projects of Key Disciplines of Guangdong Province (2022ZDJS141), Key Research Platforms and Projects of Universities of Guangdong Province (2022ZDZX3039), Guangdong Provincial Engineering Technology Research Center of the Green Polyurethane Adhesives, Zhuhai College of Science and Technology (2021GCZX010), the Innovative School Project of Education Department of Guangdong (2021KQNCX145), and Science Foundation of Faculty of Comprehensive Health Industry (2023DJKCY013).

References

1 B. Kumar, M. Llorente, J. Froehlich, T. Dang, A. Sathrum and C. P. Kubiak, Photochemical and Photoelectrochemical Reduction of CO_2, *Annu. Rev. Phys. Chem.*, 2012, **63**, 541–569.
2 A. Goeppert, M. Czaun, J.-P. Jones, G. K. S. Prakash and G. A. Olah, Recycling of carbon dioxide to methanol and derived products - closing the loop, *Chem. Soc. Rev.*, 2014, **43**(23), 7995–8048.
3 M. Mikkelsen, M. Jorgensen and F. C. Krebs, The teraton challenge. A review of fixation and transformation of carbon dioxide, *Energy Environ. Sci.*, 2010, **3**(1), 43–81.
4 W. H. Zhang, A. R. Mohamed and W. J. Ong, Z-Scheme Photocatalytic Systems for Carbon Dioxide Reduction: Where Are We Now?, *Angew. Chem., Int. Ed.*, 2020, **59**(51), 22894–22915.
5 L. J. Liu, H. L. Zhao, J. M. Andino and Y. Li, Photocatalytic CO2 Reduction with H2O on TiO2 Nanocrystals: Comparison of Anatase, Rutile, and Brookite Polymorphs and Exploration of Surface Chemistry, *ACS Catal.*, 2012, **2**(8), 1817–1828.
6 W. L. Yu, D. F. Xu and T. Y. Peng, Enhanced photocatalytic activity of g-C3N4 for selective CO2 reduction to CH3OH via facile coupling of ZnO: a direct Z-scheme mechanism, *J. Mater. Chem. A*, 2015, **3**(39), 19936–19947.
7 J. Jin, J. G. Yu, D. P. Guo, C. Cui and W. K. Ho, A Hierarchical Z-Scheme CdS-WO3 Photocatalyst with Enhanced CO2 Reduction Activity, *Small*, 2015, **11**(39), 5262–5271.
8 C. Han, J. Li, Z. Ma, H. Xie, G. I. N. Waterhouse, L. Ye and T. Zhang, Black phosphorus quantum dot/g-C3N4 composites for enhanced CO2 photoreduction to CO, *Sci. China Mater.*, 2018, **61**(9), 1159–1166.
9 Y. F. Zhao, G. B. Chen, T. Bian, C. Zhou, G. I. N. Waterhouse, L. Z. Wu, C. H. Tung, L. J. Smith, D. O'Hare and T. R. Zhang, Defect- Rich Ultrathin ZnAl-Layered Double Hydroxide Nanosheets for Efficient Photoreduction of CO2 to CO with Water, *Adv. Mater.*, 2015, **27**(47), 7824–7831.
10 J. Ke, M. A. Younis, Y. Kong, H. R. Zhou, J. Liu, L. C. Lei and Y. Hou, Nanostructured Ternary Metal Tungstate-Based Photocatalysts for Environmental Purification and Solar Water Splitting: A Review, *Nano-Micro Lett.*, 2018, **10**(4), 69.
11 F. Li, L. Zhang, J. C. Tong, Y. L. Liu, S. G. Xu, Y. Cao and S. K. Cao, Photocatalytic CO2 conversion to methanol by Cu2O/graphene/TNA heterostructure catalyst in a visible-light-driven dual-chamber reactor, *Nano Energy*, 2016, **27**, 320–329.
12 J. H. Peng, X. Z. Chen, W. J. Ong, X. J. Zhao and N. Li, Surface and Heterointerface Engineering of 2D MXenes and Their Nanocomposites: Insights into Electro- and Photocatalysis, *Chem*, 2019, **5**(1), 18–50.
13 J. C. Wang, H. C. Yao, Z. Y. Fan, L. Zhang, J. S. Wang, S. Q. Zang and Z. J. Li, Indirect Z-Scheme BiOl/g-C3N4 Photocatalysts with Enhanced Photoreduction CO2 Activity under Visible Light Irradiation, *ACS Appl. Mater. Interfaces*, 2016, **8**(6), 3765–3775.
14 C. B. Hiragond, J. Lee, H. Kim, J. W. Jung, C. H. Cho and S. I. In, A novel N-doped graphene oxide enfolded reduced titania for highly stable and selective gas-phase photocatalytic CO2 reduction into CH4: an in-depth study on the interfacial charge transfer mechanism, *Chem. Eng. J.*, 2021, **416**, 127978.
15 J. Y. Hao, B. J. Qi, J. J. Wei, D. Li and F. Y. Zeng, A Z-scheme Cu2O/WO3 heterojunction for production of renewable hydrocarbon fuel from carbon dioxide, *Fuel*, 2021, **287**, 119439.
16 C. B. Bie, B. C. Zhu, F. Y. Xu, L. Y. Zhang and J. G. Yu, In Situ Grown Monolayer N-Doped Graphene on CdS Hollow Spheres with Seamless Contact for Photocatalytic CO2 Reduction, *Adv. Mater.*, 2019, **31**(42), 1902868.
17 F. Y. Tian, H. L. Zhang, S. Liu, T. Wu, J. H. Yu, D. H. Wang, X. B. Jin and C. Peng, Visible-light-driven CO2 reduction to ethylene on CdS: Enabled by structural relaxation-induced intermediate dimerization and enhanced by ZIF-8 coating, *Appl. Catal., B*, 2021, **285**, 119834.
18 L. Pei, Y. J. Yuan, W. F. Bai, T. Z. Li, H. Zhu, Z. F. Ma, J. S. Zhong, S. C. Yan and Z. G. Zou, In Situ-Grown Island-

Shaped Hollow Graphene on TaON with Spatially Separated Active Sites Achieving Enhanced Visible-Light CO2 Reduction, *ACS Catal.*, 2020, **10**(24), 15083–15091.

19 Y. G. Wang, F. Wang, Y. T. Chen, D. F. Zhang, B. Li, S. F. Kang, X. Li and L. F. Cui, Enhanced photocatalytic performance of ordered mesoporous Fe-doped CeO2 catalysts for the reduction of CO2 with H2O under simulated solar irradiation, *Appl. Catal., B*, 2014, **147**, 602–609.

20 Y. M. He, L. H. Zhang, M. H. Fan, X. X. Wang, M. L. Walbridge, Q. Y. Nong, Y. Wu and L. H. Zhao, Z-scheme SnO2-x/g-C3N4 composite as an efficient photocatalyst for dye degradation and photocatalytic CO2 reduction, *Sol. Energy Mater. Sol. Cells*, 2015, **137**, 175–184.

21 L. Y. Zhu, H. Li, Q. L. Xu, D. H. Xiong and P. F. Xia, High-efficient separation of photoinduced carriers on double Z-scheme heterojunction for superior photocatalytic CO2 reduction, *J. Colloid Interface Sci.*, 2020, **564**, 303–312.

22 Y. M. He, L. H. Zhang, B. T. Teng and M. H. Fan, New Application of Z-Scheme Ag3PO4/g-C3N4 Composite in Converting CO2 to Fuel, *Environ. Sci. Technol.*, 2015, **49**(1), 649–656.

23 Y. Huo, J. F. Zhang, K. Dai, Q. Li, J. L. Lv, G. P. Zhu and C. H. Liang, All-solid-state artificial Z-scheme porous g-C3N4/Sn2S3-DETA heterostructure photocatalyst with enhanced performance in photocatalytic CO2 reduction, *Appl. Catal., B*, 2019, **241**, 528–538.

24 X. Li, X. H. Song, C. C. Ma, Y. L. Cheng, D. Shen, S. M. Zhang, W. K. Liu, P. W. Huo and H. Q. Wang, Direct Z-Scheme WO3/Graphitic Carbon Nitride Nanocomposites for the Photoreduction of CO2, *ACS Appl. Nano Mater.*, 2020, **3**(2), 1298–1306.

25 L. Xin, W. Jiuqing, L. Jingxiang, F. Yueping and Y. Jiaguo, Design and fabrication of semiconductor photocatalyst for photocatalytic reduction of CO 2 to solar fuel, *Sci. China Mater.*, 2014, 70–100.

26 G. W. Michael, L. W. Emily, R. M. James, W. B. Shannon, M. Qixi, A. S. Elizabeth and S. L. Nathan, Solar Water Splitting Cells, *Chem. Rev.*, 2010, 6446–6473.

27 K. Ikeue, H. Yamashita, M. Anpo and T. Takewaki, Photocatalytic reduction of CO2 with H2O on Ti−β zeolite photocatalysts: effect of the hydrophobic and hydrophilic properties, *J. Phys. Chem. B*, 2001, **105**(35), 8350–8355.

28 Y. Hori, A. Murata and R. Takahashi, Formation of hydrocarbons in the electrochemical reduction of carbon dioxide at a copper electrode in aqueous solution, *J. Chem. Soc., Faraday Trans. 1*, 1989, **85**(8), 2309–2326.

29 J. L. Lin, Z. M. Pan and X. C. Wang, Photochemical Reduction of CO2 by Graphitic Carbon Nitride Polymers, *ACS Sustain. Chem. Eng.*, 2014, **2**(3), 353–358.

30 J. S. Zhang, G. G. Zhang, X. F. Chen, S. Lin, L. Mohlmann, G. Dolega, G. Lipner, M. Antonietti, S. Blechert and X. C. Wang, Co-Monomer Control of Carbon Nitride Semiconductors to Optimize Hydrogen Evolution with Visible Light, *Angew. Chem., Int. Ed.*, 2012, **51**(13), 3183–3187.

31 Y. Pan, X. Yuan, L. Jiang, H. Yu, J. Zhang, H. Wang, R. Guan and G. Zeng, Recent advances in synthesis, modification and photocatalytic applications of micro/nano-structured zinc indium sulfide, *Chem. Eng. J.*, 2018, **354**, 407–431.

32 N. Luo, T. Montini, J. Zhang, P. Fornasiero, E. Fonda, T. Hou, W. Nie, J. Lu, J. Liu, M. Heggen, L. Lin, C. Ma, M. Wang, F. Fan, S. Jin and F. Wang, Visible-light-driven coproduction of diesel precursors and hydrogen from lignocellulose-derived methylfurans, *Nat. Energy*, 2019, **4**(7), 575–584.

33 G. Yang, H. Ding, D. Chen, J. Feng, Q. Hao and Y. Zhu, Construction of urchin-like ZnIn2S4-Au-TiO2 heterostructure with enhanced activity for photocatalytic hydrogen evolution, *Appl. Catal., B*, 2018, **234**, 260–267.

34 M. F. Kuehnel, K. L. Orchard, K. E. Dalle and E. Reisner, Selective Photocatalytic CO2 Reduction in Water through Anchoring of a Molecular Ni Catalyst on CdS Nanocrystals, *J. Am. Chem. Soc.*, 2017, **139**(21), 7217–7223.

35 Y. Peng, S. Kang and Z. F. Hu, Pt Nanoparticle-Decorated CdS Photocatalysts for CO2 Reduction and H-2 Evolution, *ACS Appl. Nano Mater.*, 2020, **3**(9), 8632–8639.

36 Q. Q. Bi, J. W. Wang, J. X. Lv, J. Wang, W. Zhang and T. B. Lu, Selective Photocatalytic CO2 Reduction in Water by Electrostatic Assembly of CdS Nanocrystals with a Dinuclear Cobalt Catalyst, *ACS Catal.*, 2018, **8**(12), 11815–11821.

37 D. C. Jiang, Z. J. Sun, H. X. Jia, D. P. Lu and P. W. Du, A cocatalyst-free CdS nanorod/ZnS nanoparticle composite for high-performance visible-light-driven hydrogen production from water, *J. Mater. Chem. A*, 2016, **4**(2), 675–683.

38 S. Xie, Z. Shen, J. Deng, P. Guo, Q. Zhang, H. Zhang, C. Ma, Z. Jiang, J. Cheng, D. Deng and Y. Wang, Visible light-driven C−H activation and C–C coupling of methanol into ethylene glycol, *Nat. Commun.*, 2018, **9**(1), 1181.

39 A. Datta, S. K. Panda and S. Chaudhuri, Synthesis and optical and electrical properties of CdS/ZnS Core/Shell nanorods, *J. Phys. Chem. C*, 2007, **111**(46), 17260–17264.

40 J. S. Hammond, S. W. Gaarenstroom and N. Winograd, X-Ray Photoelectron Spectroscopic Studies of Cadmium-Oxygen and Silver-Oxygen Surfaces, *Anal. Chem.*, 1975, **47**(13), 2193–2199.

41 D. W. Wakerley, M. F. Kuehnel, K. L. Orchard, K. H. Ly, T. E. Rosser and E. Reisner, Solar-driven reforming of lignocellulose to H-2 with a CdS/CdOx photocatalyst, *Nat. Energy*, 2017, **2**(4), 17021.

42 B. Schreder, C. Dem, M. Schmitt, A. Materny, W. Kiefer, U. Winkler and E. Umbach, Raman spectroscopy of II-VI semiconductor nanostructures: CdS quantum dots, *J. Raman Spectrosc.*, 2003, **34**(2), 100–103.

43 R. Cusco, J. Ibanez, N. Domenech-Amador, L. Artus, J. Zuniga-Perez and V. Munoz-Sanjose, Raman scattering of cadmium oxide epilayers grown by metal-organic vapor phase epitaxy, *J. Appl. Phys.*, 2010, **107**(6), 063519.

44 B. Wang, S. He, W. H. Feng, L. L. Zhang, X. Y. Huang, K. Q. Wang, S. Y. Zhang and P. Liu, Rational design and facile in situ coupling non-noble metal Cd nanoparticles

and CdS nanorods for efficient visible-light-driven photocatalytic H-2 evolution, *Appl. Catal., B*, 2018, **236**, 233–239.

45 T. T. Hou, N. C. Luo, Y. T. Cui, J. M. Lu, L. Li, K. E. MacArthur, M. Heggen, R. T. Chen, F. T. Fan, W. M. Tian, S. Y. Jin and F. Wang, Selective reduction of CO2 to CO under visible light by controlling coordination structures of CeOx-S/ZnIn2S4 hybrid catalysts, *Appl. Catal., B*, 2019, **245**, 262–270.

46 L. Liang, X. D. Li, Y. F. Sun, Y. L. Tan, X. C. Jiao, H. X. Ju, Z. M. Qi, J. F. Zhu and Y. Xie, Infrared Light-Driven CO2 Overall Splitting at Room Temperature, *Joule*, 2018, **2**(5), 1004–1016.

47 G. Kresse and J. Furthmuller, Efficiency of ab initio total energy calculations for metals and semiconductors using a plane-wave basis set, *Comput. Mater. Sci.*, 1996, **6**(1), 15–50.

48 J. P. Perdew, K. Burke and M. Ernzerhof, Generalized gradient approximation made simple, *Phys. Rev. Lett.*, 1996, **77**(18), 3865–3868.

49 G. Kresse and D. Joubert, From ultrasoft pseudopotentials to the projector augmented-wave method, *Phys. Rev. B: Condens. Matter Mater. Phys.*, 1999, **59**, 1758–1775.

50 H. J. Monkhorst and J. D. Pack, Special Points for Brillouin-Zone Integrations, *Phys. Rev. B: Solid State*, 1976, **13**(12), 5188–5192.

51 J. S. Jang, U. A. Joshi and J. S. Lee, Solvothermal synthesis of CdS nanowires for photocatalytic hydrogen and electricity production, *J. Phys. Chem. C*, 2007, **111**(35), 13280–13287.